Original Article

CT imaging-based nomogram for predicting pleural invasion in non-small cell lung cancer

Jinsong Bai^{1*}, Haibo Wang^{2*}, Chi Zhang¹, Hongying Li¹, Qian Zhu¹, Zhao Hou¹, Jingyi Huang¹, Haitao Zhang¹

¹Department of Medical Imaging, Hanzhong People's Hospital, Hanzhong 723000, Shaanxi, China; ²Department of Medical Imaging, The Second Affiliated Hospital of Harbin Medical University, Harbin 150000, Heilongjiang, China. *Co-first authors.

Received July 4, 2025; Accepted August 25, 2025; Epub September 15, 2025; Published September 30, 2025

Abstract: Objective: To identify risk factors for visceral pleural invasion (VPI) in non-small cell lung cancer (NSCLC) using preoperative CT characteristics and develop a nomogram for VPI prediction. Methods: We collected clinical data from 282 NSCLC patients (July 2020-June 2022) who underwent CT scans. Patients were categorized into VPI (n=70) and non-VPI (n=212) groups. Demographic, pathologic, and CT characteristics were analyzed. Logistic regression was applied to identify VPI-related determinants, and a nomogram was developed. Diagnostic performance was assessed using receiver operating characteristic (ROC) curves, decision curve analysis (DCA), and calibration curves. Results: No significant differences were observed between the groups for gender, age, BMI, disease duration, KPS score, smoking/alcohol history, tumor location, pathologic type, or CT features (all P>0.05). The VPI group had higher proportions of moderately/poorly differentiated tumors, advanced N-stage, M1-stage, larger tumor size, pleural retraction, pleura-adherence, and irregular morphology (all P<0.05). Multivariate analysis identified significant predictors: moderate/poor differentiation (OR=2.41), N2-N3 stage (OR=3.17), M1 stage (OR=2.89), pleural retraction (OR=4.02), pleura adherence (OR=3.55), irregular morphology (OR=3.21), and larger tumor diameter (OR=1.98) (all P<0.05). The model exhibited AUCs of 0.933 (training) and 0.959 (validation). Bootstrap validation (B=1000) indicated good calibration. The VPI group had a lower 3-year survival rate (69.57%) compared to the non-VPI group (80.66%) (P<0.05). Conclusion: VPI in NSCLC is associated with worse prognosis. The CT features, including pleural indentation and irregular morphology, may be used to predict VPI. The nomogram developed will be a valuable tool for clinical decision-making and improving patient outcomes.

Keywords: Non-small cell lung carcinoma, visceral pleural invasion, computed tomography, radiologic characteristics, nomogram

Introduction

Non-small cell lung cancer (NSCLC), the most common histologic subtype of pulmonary cancer, accounts for over 85% of new cases and has a 5-year survival rate ranging from 12% to 15% [1]. Due to the absence of typical symptoms in early-stage NSCLC and its aggressive nature, approximately 70% of patients are diagnosed at an advanced stage, missing the optimal time for surgery, which significantly shortens their survival [2]. Thus, improving early diagnosis and accurate staging of NSCLC is critical for enhancing patient prognosis and survival. Among the key factors influencing NSCLC staging and prognosis, visceral pleural invasion (VPI) stands out as a critical indepen-

dent prognostic indicator [3]. VPI refers to tumor invasion of the elastic layer of the visceral pleura or its surface, and it is crucial for T-stage upstaging. According to the TNM staging criteria established by the International Association for the Study of Lung Cancer (IA-SLC) and the Union for International Cancer Control (UICC), the presence of VPI mandates the upstaging of a tumor initially classified as pathologic T1 (≤3 cm in diameter and confined to the lung parenchyma) to stage IB (pathologic T2a), significantly reducing the patient's 5-year survival [4]. International studies have identified VPI as an independent risk factor for postoperative recurrence, pleural seeding, and distant metastasis in NSCLC patients [5]. Therefore, early identification of individuals at high

risk for VPI is essential for guiding personalized surgical strategy, such as more extensive resection margins and systematic lymph node dissection, ultimately improving patient outcome. The diagnosis of VPI primarily relies on postoperative pathologic examination, which, though the gold standard, is invasive and subject to diagnostic delay, thus complicating preoperative clinical decision-making. At present, there is a lack of simple, non-invasive preoperative predictive methods.

Computed tomography (CT) plays a vital role in diagnosing NSCLC, providing detailed information on suspicious pulmonary lesions, lesion morphology, relationships to surrounding tissues, and lung structure. While CT offers valuable anatomic data, conventional approaches using isolated imaging signs (e.g., pleural retraction or thickening) for predicting VPI often lack specificity due to tumor heterogeneity [6, 7]. These features can be caused by factors other than tumor invasion, such as inflammation or fibrosis, and the absence of standardized quantitative criteria leads to low diagnostic sensitivity and accuracy [8]. The nomogram, a visual predictive tool, integrates multiple clinical predictors, including demographic and laboratory data, to enhance individualized risk stratification and improve clinical risk assessment [9]. Despite reports on factors associated with VPI in NSCLC, the lack of standardized quantitative models has hindered the development of robust prediction [10, 11]. This study aimed to analyze factors influencing VPI in NSCLC patients and construct a nomogram predictive model based on CT imaging characteristics, providing a foundation for precise diagnosis, personalized treatment, and improved patient survival.

Materials and methods

Patient selection

We initially selected 290 NSCLC patients who were treated at our hospital between July 2020 and June 2022 through the electronic medical record (EMR) system.

Inclusion criteria: (1) Histopathologic confirmation of NSCLC post-resection; (2) No preoperative targeted therapy, radiotherapy, or neoadjuvant therapy; (3) CT scan performed within 2

weeks prior to surgery; (4) Complete clinical data.

Exclusion criteria: (1) III-defined lesion margins adjacent to major vasculature on CT; (2) Suboptimal CT image quality preventing accurate lesion segmentation; (3) New York Heart Association (NYHA) Class III-IV congestive heart failure; (4) Inadequate pleural status documentation in pathology reports; (5) Concurrent primary malignancy; (6) Arterial thromboembolic events within 6 months prior to enrollment; (7) Severe uncontrolled infection; (8) Active pulmonary tuberculosis or primary immunodeficiency disorders; (9) Interstitial lung disease (ILD).

Of the 290 NSCLC patients, 2 were excluded due to a CT-surgery interval exceeding two weeks, 1 due to poor CT image quality, 2 for incomplete follow-up data, and 3 for lack of clear pleural status description in postoperative pathology. Ultimately, 282 patients were included in the study. This research was approved by the Ethics Committee of Hanzhong People's Hospital (approval reference: BF 2024-05-26). The selection flowchart is shown in **Figure 1**.

Data acquisition

Data extraction was conducted through the EMR system to gather preoperative clinical data, including age, sex, body mass index (BMI), disease duration, smoking history, alcohol consumption history, Karnofsky Performance Status (KPS) score, tumor location (peripheral or central), pathologic type (adenocarcinoma, squamous cell carcinoma, large cell carcinoma), differentiation grade (moderately/ poorly differentiated or well-differentiated), N stage (NO-N1 or N2-N3), M stage (MO or M1), and tumor diameter. Preoperative CT imaging features were also extracted, such as lesion lobe distribution (left upper lobe, left lower lobe, right upper lobe, right middle lobe, right lower lobe), spiculation sign, cavitation sign, lobulation sign, subpleural effusion, air bronchogram sign, vascular bundle sign, pleural indentation sign, tumor abutting the chest wall, and tumor shape characteristics (regular or irregular).

Postoperative data included survival rate, with a follow-up cutoff date of June 2025. The date

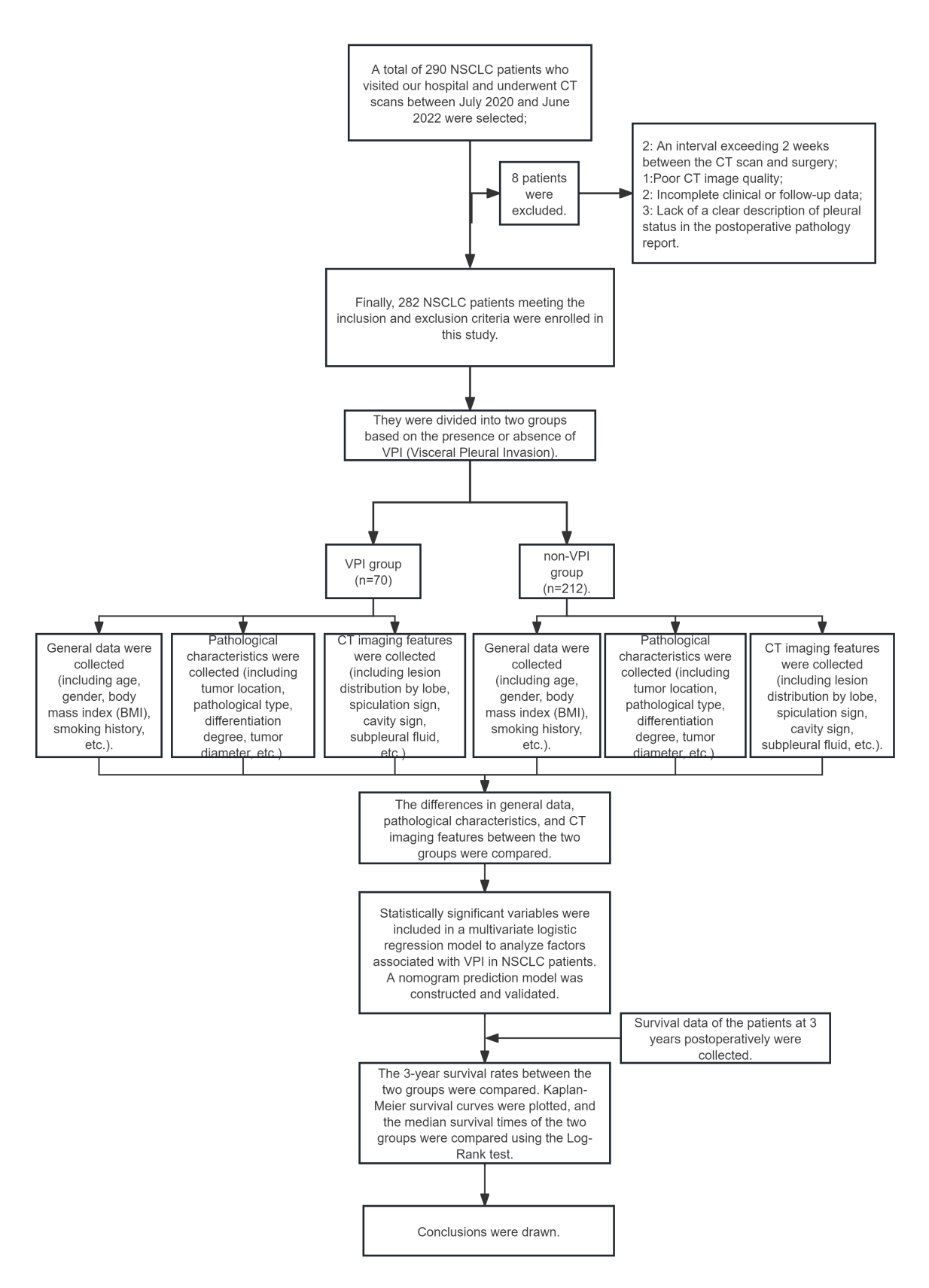


Figure 1. Flow chart.

Table 1. Comparison of general information between the two groups

Group	n	Male/ Female	Age (years)	BMI (kg/m²)	Disease duration (years)	History of smoking	History of alcohol consumption	KPS score (points)
non-VPI group	212	126/86	60.38±5.58	23.74±2.08	5.25±1.15	108	94	84.26±5.02
VPI group	70	43/27	60.97±4.87	24.13±1.98	5.49±1.37	37	30	83.16±4.88
χ^2/t		0.087	0.791	1.376	1.441	0.077	0.047	1.601
Р		0.768	0.430	0.170	0.151	0.781	0.829	0.111

of death served as the endpoint for deceased patients, while censored data included patients still alive at follow-up cutoff, deaths from other causes or accidents, and those lost to follow-up. VPI was determined according to the International Association for the Study of Lung Cancer (IASLC) 8th edition TNM staging system [12] and pathologic findings. VPI was diagnosed directly if pleural invasion was microscopically evident. Special elastic fiber staining was used for confirmation in sections adjacent to the pleura without obvious invasion signs. Patients with VPI were assigned to the VPI group, while others were categorized into the non-VPI group.

End result indicators

Main indicators: Comparison of preoperative CT imaging characteristics between the VPI and non-VPI groups.

Secondary indicators: Comparison of preoperative clinical data, pathological types, and 3-year postoperative survival rates between the VPI and non-VPI groups.

Statistical analysis

Statistical analysis was performed using SPSS 26.0. A normality test was conducted for all measured data. For data following a normal distribution, independent sample t-tests were applied, with results expressed as mean ± standard deviation ($\bar{x} \pm sd$). Counted data were presented as percentages and analyzed using the x² test. The relationship between CT imaging characteristics and VPI occurrence was assessed using the Phi coefficient correlation. A multivariate logistic regression model was used to identify variables affecting VPI in NSCLC patients. The nomogram predictive model for VPI was developed using R software's "rms" package. The model's predictive effectiveness was evaluated using the ROC curve, clinical decision curve, and calibration curve. Survival rates were calculated using the Kaplan-Meier survival function. Statistical significance was set at P<0.05.

Results

General information in the two groups

The cohort included 169 male and 113 female participants, aged 43 to 73 years, with an average age of 60.52±5.11 years. Their body mass index (BMI) ranged from 20.15 to 27.65 kg/m², with an average of 23.89±2.05 kg/m². Disease duration ranged from 2 to 9 years, with an average of 5.38±1.24 years. Of the participants, 145 had a history of smoking, and 124 had a history of alcohol consumption. No significant differences were observed between the two groups in terms of gender, age, BMI, KPS score, disease duration, smoking history, and alcohol consumption history (all P>0.05) (**Table 1**).

Comparison of pathologic characteristics between the two groups

The VPI group had higher proportions of poorly differentiated tumors, advanced N stage, advanced M stage, and larger tumor diameter compared to the non-VPI group (all P<0.05) (Table 2).

Comparison of CT imaging features between the two groups

The VPI group showed significantly higher proportions of pleural indentation sign, tumor abutment to the chest wall, and irregular lesion shape compared to the non-VPI group (all P<0.05) (**Table 3**). Phi coefficient correlation analysis revealed significant correlations between pleural indentation sign (r=0.167, P= 0.005), tumor abutting the chest wall (r=0.230, P,0.001), and irregular tumor shape (r=0.273, P<0.001) with the occurrence of VPI.

Table 2. Comparison of pathologic characteristics between the two groups

Feature		VPI group (n=70)	non-VPI group (n=212)	χ^2/t	Р
Tumor location	Peripheral type	38 (24.29)	111 (52.36)	0.078	0.780
	Central type	32 (45.71)	101 (47.64)		
Pathological type	Adenocarcinoma	34 (48.57)	102 (48.11)	0.277	0.871
	Squamous cell carcinoma	24 (34.29)	68 (32.08)		
	Large cell carcinoma	12 (17.14)	42 (19.81)		
Differentiation	Moderately and poorly differentiated	38 (54.29)	39 (18.40)	34.149	0.000
grade	Highly differentiated	32(45.71)	173 (81.60)		
N stage	NO-N1	18 (25.71)	145 (68.40)	39.304	0.000
	N2-N3	52 (74.29)	67 (31.60)		
M stage	MO	20 (28.57)	106 (50.00)	9.776	0.002
	M1	50 (71.43)	106 (50.00)		
Tumor diameter (d	cm)	5.49±1.15	3.58±0.95	13.814	0.000

Table 3. Comparison of CT imaging characteristics between the two groups

Feature		VPI group (n=70)	non-VPI group (n=212)	χ²	Р
Distribution of lesion in lung lobes	The upper lobe of the left lung	11 (15.71)	42 (19.81)	0.516	0.425
	The lower lobe of the left lung	15 (21.43)	55 (25.94)		
	Right upper lobe of the lung	22 (31.43)	65 (30.66)		
	Middle lobe of the right lung	5 (7.14)	12 (5.66)		
	The lower lobe of the right lung	17 (24.29)	38 (17.92)		
The burr sign	Yes	34 (48.57)	99 (46.70)	0.074	0.786
	No	36 (51.43)	113 (53.30)		
Cavity sign	Yes	16 (22.86)	37 (17.45)	1.007	0.316
	No	54 (77.14)	175 (82.55)		
Lobulation sign	Yes	28 (40.00)	78 (36.79)	0.231	0.631
	No	42 (60.00)	134 (63.21)		
Subpleural effusion	Yes	20 (28.57)	61 (28.77)	0.001	0.934
	No	50 (71.43)	151 (71.23)		
Bronchial air sign	Yes	15 (21.43)	39 (18.40)	0.313	0.576
	No	55 (78.57)	173 (81.60)		
Cluster of blood vessels sign	Yes	13 (18.57)	40 (18.87)	0.003	0.956
	No	57 (81.43)	172 (81.13)		
Pleural indentation sign	Yes	31 (44.29)	56 (26.43)	7.878	0.005
	No	39 (55.71)	156 (73.58)		
Tumor abutment to the chest wall	Yes	41 (58.57)	69 (32.55)	14.980	0.000
	No	29 (41.43)	143 (67.48)		
Lesion shape characteristics	Regular	29 (41.43)	152 (71.70)	20.975	0.000
	Irregular	41 (58.57)	60 (28.30)		

Multivariate logistic regression analysis of NSCLC patients with VPI

A multivariate logistic regression model was developed with the presence of VPI in NSCLC patients (0 = no, 1 = yes) as the dependent vari-

able and significant indicators from **Tables 2** and **3** as independent variables (values assigned as shown in **Table 4**). The backward stepwise regression method (Backward: LR) was used with an exclusion criterion of P> 0.10. The analysis revealed that factors such

Table 4. Assignment of main independent variables

Independent variable	Variable Description	Assignment Instructions
Differentiation grade	Categorical variable	Low and moderate differentiation = 1, high differentiation = 0
N stage	Categorical variable	N2-N3 = 1, $N0-N1 = 0$
M stage	Categorical variable	M1 = 1, $MO = 0$
Pleural indentation sign	Categorical variable	Yes = 1, No = 0
Tumor abutment to the chest wall	Categorical variable	Yes = 1, No = 0
Lesion morphology	Categorical variable	Yes = 1, No = 0
Tumor diameter	Continuous variable	Original value entry

Table 5. Single factor Logistic regression analysis of NSCLC patients with VPI

Factor	В	SE	Wald	Р	OR	95% CI
Differentiation grade	1.842	0.275	44.821	0.000	6.310	3.682-10.815
N stage	1.913	0.285	45.122	0.000	6.775	3.876-11.842
M stage	0.865	0.273	10.054	0.002	2.375	1.392-4.053
Pleural indentation sign	1.402	0.288	23.710	0.000	4.062	2.310-7.142
Tumor abutment to the chest wall	1.182	0.265	19.892	0.000	3.262	1.940-5.486
Lesion morphology	1.325	0.274	23.381	0.000	3.763	2.199-6.439
Tumor diameter	0.892	0.098	82.913	0.000	2.440	2.012-2.959

Table 6. Multivariate logistic regression analysis of NSCLC patients with VPI

Factor	В	SE	Wald	Р	OR	95% CI
Differentiation grade	1.662	0.298	31.025	0.000	5.268	2.936-9.452
N stage	1.833	0.311	34.775	0.000	6.252	3.400-11.497
M stage	0.727	0.298	5.937	0.015	2.069	1.153-3.713
Pleural indentation sign	1.357	0.302	20.168	0.000	3.886	2.149-7.027
Tumor abutment to the chest wall	1.075	0.283	14.381	0.000	2.930	1.681-5.107
Lesion morphology	1.276	0.287	19.821	0.000	3.582	2.042-6.281
Tumor diameter	1.823	0.229	63.644	0.000	6.190	3.955-9.687
Constant	-9.615	1.284	54.683	0.000	0.000	-

as moderate to low differentiation, N2-N3 stage, M1 stage, pleural indentation sign, tumor abutting the chest wall, irregular tumor shape, and larger tumor diameter were significant risk factors for VPI in NSCLC patients (OR>1, P<0.05) (Tables 5 and 6).

Construction of a nomogram predictive model for NSCLC patients with VPI and evaluation of predictive performance

A nomogram was constructed based on the multivariate logistic regression results to quantify independent risk factors for VPI (**Figure 2**). The predictive ability of the model was evaluated using the ROC curve (**Figure 3**). The model showed an AUC of 0.933 (95% CI: 0.888-0.977) in the training set and 0.959

(95% CI: 0.920-0.999) in the validation set (**Table 7**).

Clinical application value

In the clinical decision curves for both the training and validation sets, the net benefit of the predictive model was greater than 0, positioned above the two null lines. This indicates that the predictive model provides a relatively high net benefit (**Figure 4**).

Internal validation of the predictive model

The Bootstrap method (B=1000) was used for internal validation of the predictive model. The calibration curve closely matched the ideal curve. The model's predictive capacity was

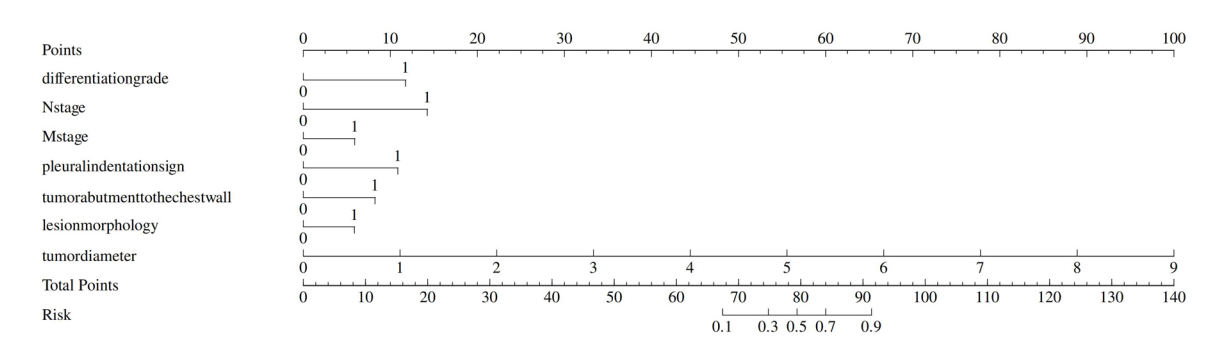


Figure 2. Nomogram prediction model.

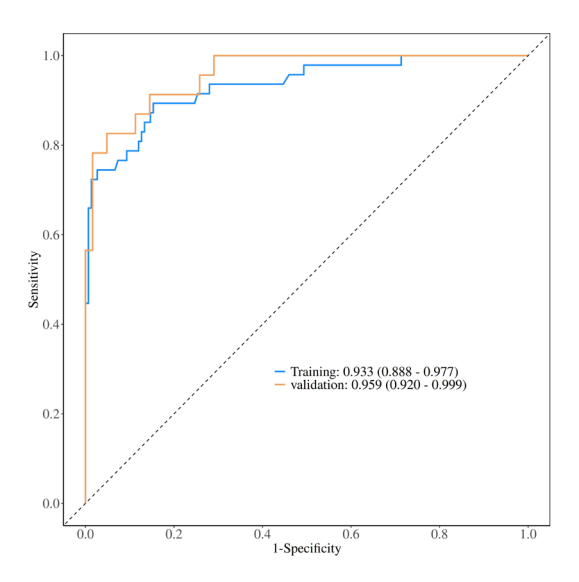


Figure 3. ROC curves of the training set and validation set models.

demonstrated by the training set's C-index of 0.758 (P=0.599) and the validation set's C-index of 0.892 (P=0.992) (**Figure 5**).

Comparison of prognosis between groups

There were no significant differences in the 1-year and 2-year survival rates between the VPI and non-VPI groups (P>0.05). However, the 3-year survival rate was significantly lower in the VPI group (69.57%) compared to the non-VPI group (80.66%) (P<0.05, **Table 8**). The median survival times for the VPI and non-VPI groups were 31.500 months (95% CI: 29.583-33.417) and 33.137 months (95% CI: 32.188-34.086), respectively. The log-rank test showed that the median survival time during the 3-year follow-up was significantly shorter in the VPI group (χ^2 =4.474, P=0.034, **Figure 6**).

Representative case analysis

A 69-year-old male with poorly differentiated squamous cell carcinoma in the right upper lobe and pleural invasion. Axial lung window: Irregularly shaped tumor abutting the chest wall, displaying lobulation, spiculation, and vascular convergence sign (Figure 7A). Axial mediastinal window: Ill-defined interface between the tumor and pleura (Figure 7B). Coronal mediastinal window: Pleural indentation with obscured tumor-pleural boundary (Figure 7C).

A 53-year-old male with well-differentiated adenocarcinoma in the right upper lobe and no pleural invasion. Features: Regularly shaped tumor with smooth margins, vascular convergence sign, and pleural indentation sign; clear separation from the chest wall. Axial lung window (Figure 8A), Axial mediastinal window (Figure 8B), Coronal mediastinal window (Figure 8C).

Discussion

The visceral pleura is a serous membrane that envelops the pulmonary surface. Tumor penetration beyond this layer indicates the breach of an anatomic boundary and invasion into the pleural space. In the randomized non-inferiority CALGB 140503 trial (Alliance for Clinical Trials in Oncology) involving 697 T1NO NSCLC patients, VPI was identified in 113 cases (16.21%) and independently predicted increased recurrence (HR=1.89, P=0.002) and mortality (HR=1.76, P=0.008) [13]. Another multicenter cohort study reported a 26.27% incidence of VPI (372/1416) among stage I-III NSCLC patients, with VPI associated with reduced overall survival (adjusted OR: 1.44, 95% CI: 1.17-1.76) [14]. Our cohort demonstrated comparable VPI prevalence (70/282,

Table 7. Evaluation of diagnostic efficiency

Data	AUC (95% CI)	Accuracy (95% CI)	Sensitivity (95% CI)	Specificity (95% CI)	PPV (95% CI)	NPV (95% CI)
Train	0.933 (0.888-0.977)	0.858 (0.801-0.903)	0.847 (0.789-0.904)	0.894 (0.805-0.982)	0.962 (0.930-0.995)	0.646 (0.530-0.762)
Test	0.959 (0.920-0.999)	0.835 (0.739-0.907)	0.806 (0.708-0.905)	0.913 (0.798-1.000)	0.962 (0.909-1.000)	0.636 (0.472-0.800)

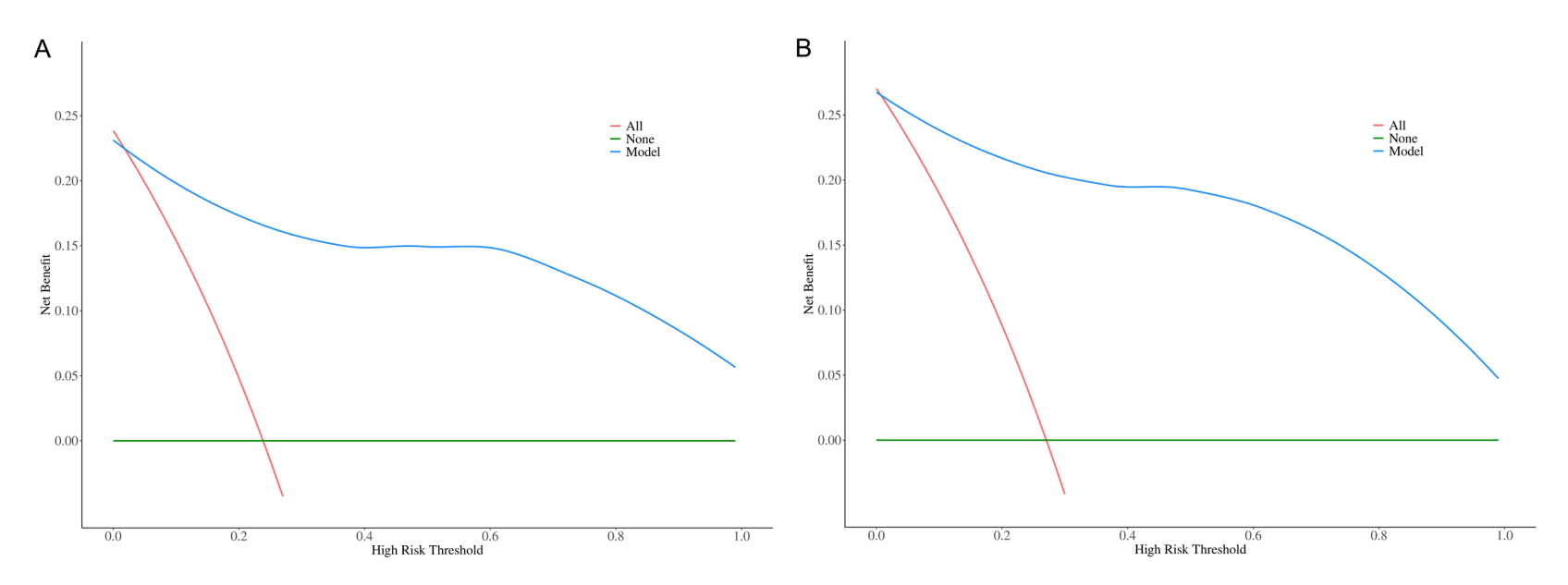


Figure 4. Clinical decision curve analysis for training and validation sets. A. Training set; B. Validation set. The horizontal axis represents the risk range of NSCLC patients with VPI predicted by the model, and the vertical axis represents clinical application value. The clinical application value is positively correlated with the area under the decision curve.

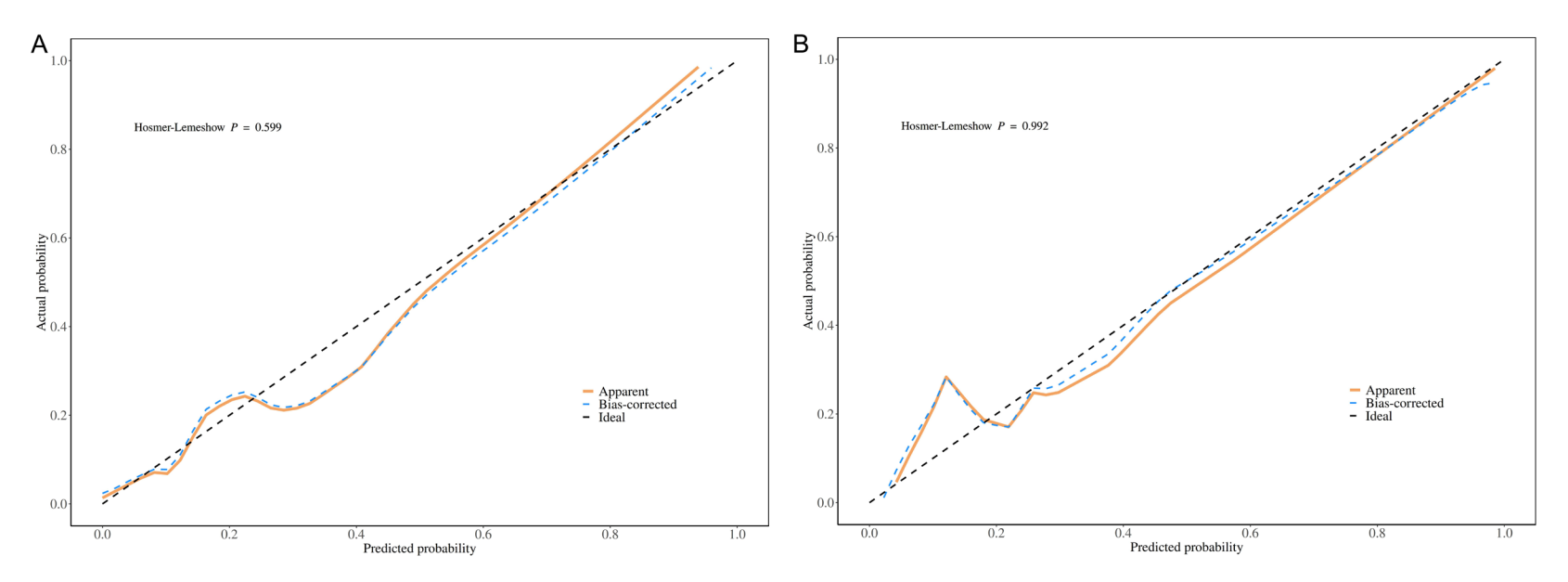


Figure 5. Calibration curves for training and validation sets. Note: A. Training set; B. Validation set. In the calibration plot, the abscissa represents the model-predicted visceral pleural invasion (VPI) probability in non-small cell lung cancer (NSCLC) patients, while the ordinate corresponds to observed probabilities. Enhanced calibration accuracy is indicated by closer alignment of the curve to the 45-degree ideal reference line.

Table 8. Comparison of overall survival rates between groups n (%)

Croup	n	1-year survival	2-year survival	3-year survival	
Group	n	rate	rate	rate	
Non-group	212	203 (95.75)	189 (89.15)	171 (80.66)	
VPI group	70	65 (92.86)	57 (81.43)	48 (69.57)	
χ^2		0.423	2.818	4.433	
Р		0.515	0.093	0.035	

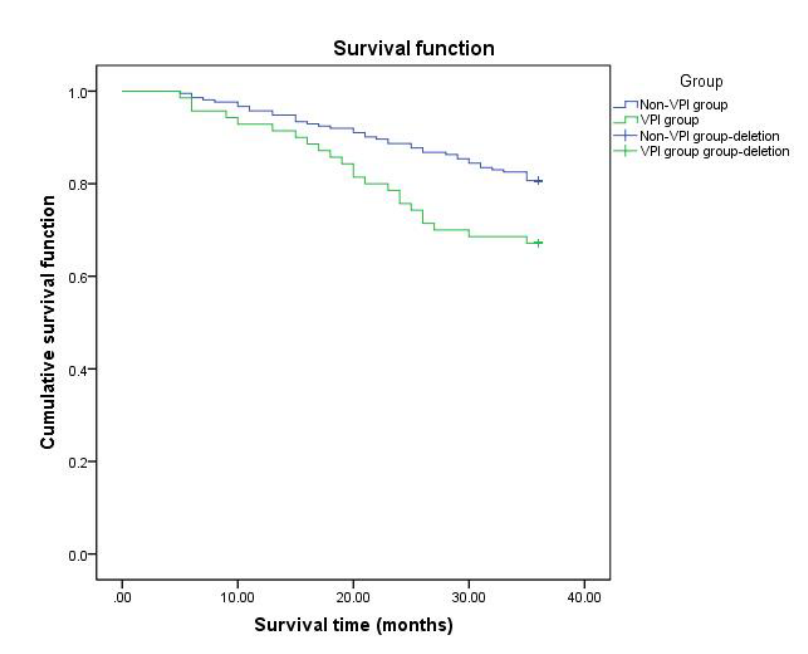


Figure 6. Survival function of VPI and non-VPI groups.

24.82%), consistent with these findings. Further analysis of follow-up data revealed that the 3-year survival rate in the VPI group (69.57%) was significantly lower than in the non-VPI group (80.66%). The median survival times for the VPI and non-VPI groups were 31.500 months (95% CI: 29.583-33.417) and 33.137 months (95% CI: 32.188-34.086), respectively. A log-rank test confirmed that the 3-year median survival time of the VPI group was significantly shorter than that of the non-VPI group (χ^2 =4.474, P=0.034), demonstrating poorer prognosis and reduced survival in NSCLC patients with visceral pleural invasion. Given its implications for extensive microscopic dissemination, VPI must be detected histologically to enable risk stratification and targeted therapy to improve survival.

Univariate and multivariate logistic regression analyses identified that moderately/poorly differentiated tumors, N2-N3 stage, M1 stage,

pleural indentation sign, tumor abutting the chest wall, irregular tumor shape, and larger tumor diameter were associated with an increased risk of visceral pleural invasion (VPI) in NSCLC patients. The elevated risk for each factor can be attributed to: Tumor cells with low or moderate differentiation lose their normal polarity and have reduced intercellular connections, allowing them to detach from the primary lesion and infiltrate surrounding tissues, thus increasing the risk of VPI [15]. Poorly differentiated lesions often grow invasively and spread along the alveolar walls to the pleura, resulting in a higher incidence of VPI. N2 stage involves metastatic involvement of ipsilateral mediastinal and/or subcarinal lymph nodes, whereas N3 designates contralateral mediastinal, hilar, or supraclavicular nodal disease. Lymph node metastasis at N2-N3 stages can impede lymphatic return, allowing tumor cells to flow retrogradely along the lymphatic

vessels to the subpleural lymphatic network and subsequently invade the visceral pleura [16]. M1 stage indicates that the tumor has spread to at least one distant site. At this stage, tumor cells can metastasize via the bloodstream to pleural microvessels, form implantation foci, and locally infiltrate, thereby increasing the risk of VPI. Pleural indentation, a linear shadow formed by thickening of the interlobular septa inside the lungs, extends from the tumor surface to the pleura. Wangetal. enrolled 140 patients with stage IA peripheral lung cancer and found a significant association between the pleural indentation sign and preoperative VPI (adjusted OR=5.08, P=0.041) [17]. Zuo et al. reported an AUC of 0.819 for a preoperative CT radiomics-based prediction model, with specificity and sensitivity of 0.757 and 0.800, respectively [18]. This study demonstrated that NSCLC patients exhibiting the pleural indentation sign on imaging had a 3.886-fold increas-





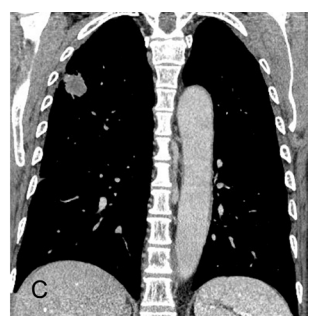
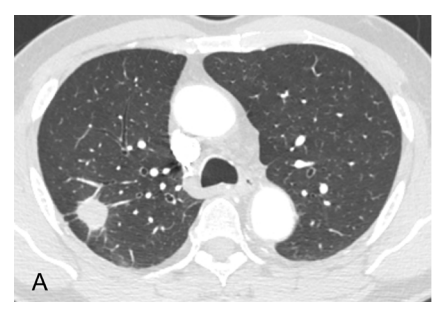


Figure 7. CT imaging features of NSCLC with VPI. Axial lung window: Irregularly shaped tumor abutting the chest wall, displaying lobulation, spiculation, and vascular convergence signs (A). Axial mediastinal window: III-defined interface between the tumor and pleura (B). Coronal mediastinal window: Pleural indentation with obscured tumor-pleural boundary (C).





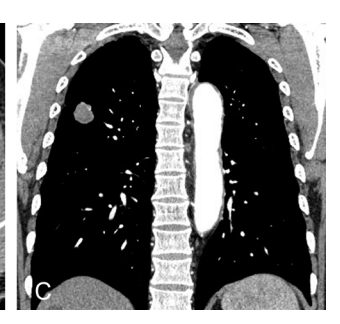


Figure 8. CT imaging features of NSCLC without VPI. Features include regularly shaped tumor with smooth margins, vascular convergence sign, and pleural indentation sign; clear separation from the chest wall. Axial lung window (A), Axial mediastinal window (B), Coronal mediastinal window (C).

ed risk (95% CI: 2.149-7.027) of concomitant VPI compared to those without this sign. This finding supports the utility of pleural indentation as a predictor for VPI. The underlying mechanism is attributed to fibrotic tissue contraction and traction within the lesion. During the initial stages, tumor cells are typically confined within the tumor core, surrounded by granulomatous infiltration or inflammatory cells. As malignant cells disrupt the interlobular septa or alveolar walls, inflammatory cells progressively accumulate around the site of invasion, leading to fibrous scar formation. The collapse of the pulmonary architecture, mediated by interstitial forces, facilitates the transmission of inflammation to the visceral pleura, causing retraction and displacement of adjacent structures, thereby generating the pleural indentation sign [19, 20]. Consequently, compared to other morphologic features, pleural indentation offers enhanced predictive utility for VPI. Lesion proximity to the chest wall is another risk factor for VPI (OR: 2.930, 95% CI: 1.681-5.107). Kong et al. reported that when the distance between

the lesion and the chest wall is ≤3 cm, the risk of pleural invasion significantly increases. If the distance is <1 cm, the risk of VPI triples, which is similar to the conclusion of this study [21]. This suggests that tumor growth exerts mechanical pressure on adjacent pleural tissue, causing ischemia and thinning of the matrix, which reduces resistance to infiltration [22]. Irregular lesion shapes reflect anisotropic tumor growth, indicating tumor cell heterogeneity and local infiltration tendencies. The irregular shape is an imaging marker of invasion into surrounding tissues [23]. Large tumor diameter generates radial mechanical pressure, promoting cell migration towards the pleura with less resistance, compressing adjacent pleural tissue, and increasing the risk of VPI. A larger tumor diameter also shortens the distance between the tumor margin and pleura, raising the incidence of VPI [24, 25].

This study integrated clinicopathologic features (differentiation grade, N/M stage) and CT imaging markers (pleural indentation, irregular

tumor shape) to construct a VPI risk prediction nomogram model, demonstrating excellent discriminative ability (C-index = 0.892). The model provides noninvasive risk assessment using seven routine indicators, overcoming limitations of single-factor predictions (e.g., low sensitivity/specificity). Its advantages of convenience, noninvasiveness, and reproducibility facilitate rapid clinical identification of highrisk VPI patients, guiding therapeutic strategy adjustments.

The CT imaging features of NSCLC patients with VPI primarily include pleural indentation, tumor proximity to the chest wall, and irregular tumor shape. The nomogram prediction model constructed based on these features should help clinicians quickly identify high-risk VPI patients and support clinical decision-making. The uniform sample collection and validation standards from a single hospital ensure the stability and consistency of testing criteria. However, the study has limitations, such as incomplete inclusion factors that may introduce biases in the data, and the model's predictive accuracy has not been verified using external data. Future research could focus on addressing these limitations.

Disclosure of conflict of interest

None.

Address correspondence to: Haitao Zhang, Department of Medical Imaging, Hanzhong People's Hospital, Room 1, Annex, No. 369, North Tujilu Street, Hanzhong 723000, Shaanxi, China. E-mail: zhang06102211@163.com

References

[1] Riely GJ, Wood DE, Ettinger DS, Aisner DL, Akerley W, Bauman JR, Bharat A, Bruno DS, Chang JY, Chirieac LR, DeCamp M, Desai AP, Dilling TJ, Dowell J, Durm GA, Gettinger S, Grotz TE, Gubens MA, Juloori A, Lackner RP, Lanuti M, Lin J, Loo BW, Lovly CM, Maldonado F, Massarelli E, Morgensztern D, Mullikin TC, Ng T, Owen D, Owen DH, Patel SP, Patil T, Polanco PM, Riess J, Shapiro TA, Singh AP, Stevenson J, Tam A, Tanvetyanon T, Yanagawa J, Yang SC, Yau E, Gregory KM and Hang L. Non-small cell lung cancer, version 4.2024, NCCN clinical practice guidelines in oncology. J Natl Compr Canc Netw 2024; 22: 249-274.

- Travis WD, Eisele M, Nishimura KK, Aly RG, Bertoglio P, Chou TY, Detterbeck FC, Donnington J, Fang W, Joubert P, Kernstine K, Kim YT, Lievens Y, Liu H, Lyons G, Mino-Kenudson M, Nicholson AG, Papotti M, Rami-Porta R, Rusch V, Sakai S, Ugalde P, Van Schil P, Yang CJ, Cilento VJ, Yotsukura M and Asamura H; Members of the International Association for the Study of Lung Cancer Staging and Prognostic Factors Committee, Members of the Advisory Boards, and Participating Institutions of the Lung Cancer Domain. The International Association for the Study of Lung Cancer (IASLC) staging project for lung cancer: recommendation to introduce spread through air spaces as a histologic descriptor in the ninth edition of the TNM classification of lung cancer. Analysis of 4061 pathologic stage I NSCLC. J Thorac Oncol 2024; 19: 1028-1051.
- [3] Minamoto F, Araújo P, D'Ambrosio P, Dela Vega A, Lauricella L, Pêgo-Fernandes P and Terra R. The association of visceral pleural invasion with skip N2 metastasis on clinical stage IA NSCLC. Clinics (Sao Paulo) 2024; 79: 100334.
- [4] Minervini F, Kestenholz P, Bertoglio P, Li A and Nilius H. Role of intrapulmonary lymph nodes in patients with NSCLC and visceral pleural invasion. The VPI 1314 multicenter registry study protocol. PLoS One 2023; 18: e0285184.
- [5] Neri S, Menju T, Sowa T, Yutaka Y, Nakajima D, Hamaji M, Ohsumi A, Chen-Yoshikawa TF, Sato T, Sonobe M, Yoshizawa A, Haga H and Date H. Prognostic impact of microscopic vessel invasion and visceral pleural invasion and their correlations with epithelial-mesenchymal transition, cancer stemness, and treatment failure in lung adenocarcinoma. Lung Cancer 2019; 128: 13-19.
- [6] Tong H, Sun J, Fang J, Zhang M, Liu H, Xia R, Zhou W, Liu K and Chen X. A machine learning model based on PET/CT radiomics and clinical characteristics predicts tumor immune profiles in non-small cell lung cancer: a retrospective multicohort study. Front Immunol 2022; 13: 859323.
- [7] Zheng J, Xu S, Wang G and Shi Y. Applications of CT-based radiomics for the prediction of immune checkpoint markers and immunotherapeutic outcomes in non-small cell lung cancer. Front Immunol 2024; 15: 1434171.
- [8] Li Z, Shi P, Qin C, Zhang W, Lin S, Zheng T, Li M and Fan L. Nomogram predicting overall survival of stage IIIB non-small-cell lung cancer patients based on the SEER database. Clin Respir J 2025; 19: e13660.
- [9] Wei SH, Zhang JM, Shi B, Gao F, Zhang ZX and Qian LT. The value of CT radiomics features to predict visceral pleural invasion in ≤3cm pe-

- ripheral type early non-small cell lung cancer. J Xray Sci Technol 2022; 30: 1115-1126.
- [10] Sun Q, Li P, Zhang J, Yip R, Zhu Y, Yankelevitz DF and Henschke Cl. CT Predictors of visceral pleural invasion in patients with non-small cell lung cancers 30 mm or smaller. Radiology 2024; 310: e231611.
- [11] Mathey-Andrews C, Abruzzo AR, Venkateswaran S, Potter AL, Senthil P, Beqari J, Yang CJ and Lanuti M. Segmentectomy vs lobectomy for early non-small cell lung cancer with visceral pleural invasion. Ann Thorac Surg 2024; 117: 1007-1014.
- [12] Nieder C, Hintz M, Oehlke O, Bilger A and Grosu AL. The TNM 8 M1b and M1c classification for non-small cell lung cancer in a cohort of patients with brain metastases. Clin Transl Oncol 2017; 19: 1141-1146.
- [13] Altorki N, Wang X, Damman B, Jones DR, Wigle D, Port J, Conti M, Ashrafi AS, Liberman M, Landreneau R, Yasufuku K, Yang S, Mitchell JD, Keenan R, Bauer T, Miller D, Kozono D, Mentlick J, Vokes E and Stinchcombe TE. Recurrence of non-small cell lung cancer with visceral pleural invasion: a secondary analysis of a randomized clinical trial. JAMA Oncol 2024; 10: 1179-1186.
- [14] Yang H and Mei T. Prognostic significance of visceral pleural invasion in patients with surgically resected small-cell lung cancer: a population-based study. Jpn J Clin Oncol 2022; 52: 1045-1055.
- [15] Zhang Y, Deng C, Zheng Q, Qian B, Ma J, Zhang C, Jin Y, Shen X, Zang Y, Guo Y, Fu F, Li H, Zheng S, Wu H, Huang Q, Wang S, Liu Q, Ye T, Sun Y, Zhang Y, Xiang J, Hu H, Li Y and Chen H. Selective mediastinal lymph node dissection strategy for clinical T1NO invasive lung cancer: a prospective, multicenter, clinical trial. J Thorac Oncol 2023; 18: 931-939.
- [16] Wightman SC, Lee JY, Ding L, Atay SM, Shemanski KA, McFadden PM, David EA and Kim AW. Adjuvant chemotherapy for visceral pleural invasion in 3-4-cm non-small-cell lung cancer improves survival. Eur J Cardiothorac Surg 2022; 62: ezab498.
- [17] Wang Y, Lyu D, Zhou T, Tu W, Fan L and Liu S. Multivariate analysis based on the maximum standard unit value of (18)F-fluorodeoxyglu-cose positron emission tomography/computed tomography and computed tomography features for preoperative predicting of visceral pleural invasion in patients with subpleural clinical stage IA peripheral lung adenocarcinoma. Diagn Interv Radiol 2023; 29: 379-389.

- [18] Zuo YQ, Gao D, Cui JJ, Yin YL, Gao ZH, Feng PY, Geng ZJ and Yang X. Peritumoral and intratumoral radiomics for predicting visceral pleural invasion in lung adenocarcinoma based on preoperative computed tomography (CT). Clin Radiol 2025; 80: 106729.
- [19] Hsu JS, Jaw TS, Yang CJ, Lin SF, Shih MP, Chou SH, Chong IW, Lin MY and Chiang IC. Convex border of peripheral non-small cell lung cancer on CT images as a potential indicator of pleural invasion. Medicine (Baltimore) 2017; 96: e7323.
- [20] Zhang Z, Zhang Q, Wang K, Zhang Z and Xu S. Risk factors and predictive efficacy of visceral pleural invasion in lung adenocarcinoma patients with mGGN type. Altern Ther Health Med 2024; 30: 46-49.
- [21] Kong X, Zhang A, Zhou X, Zhao M, Liu J, Zhang X, Zhang W, Meng X, Li N and Yang Z. A strategy for the automatic diagnostic pipeline towards feature-based models: a primer with pleural invasion prediction from preoperative PET/CT images. EJNMMI Res 2025; 15: 70.
- [22] Manyam BV, Videtic GMM, Verdecchia K, Reddy CA, Woody NM and Stephans KL. Effect of tumor location and dosimetric predictors for chest wall toxicity in single-fraction stereotactic body radiation therapy for stage I non-small cell lung cancer. Pract Radiat Oncol 2019; 9: e187-e195.
- [23] Yang Z, Li Y, Guo C, Xing Y, Liu C, Zhang J, Pu Q and Liu L. The prognostic value of visceral pleural infiltration in ≤3 cm nonsmall cell lung cancer presenting with ground glass opacity: an inverse probability of treatment weighting study. Int J Surg 2024; 110: 7871-7879.
- [24] Li L, Yang Q, Luo D, Wang X, Liu Z and Huang R. Baseline computed tomography imaging findings could assist in early diagnosis of visceral pleural invasion for newly discovered early subpleural non-small cell lung cancer: T1 or T2. J Thorac Dis 2024; 16: 5779-5791.
- [25] Ruan Z, Zhuo X and Xu C. Diagnosis, treatment, and prognosis of stage IB non-small cell lung cancer with visceral pleural invasion. Front Oncol 2023; 13: 1310471.